

A Robust INS State Initialization Method for Vehicular GNSS/MEMS-INS Integrated Navigation in Urban Environment

Jian Kuang^{id}, Longyang Ding^{id}, Yan Wang^{id}, Yilong Yuan, Pan Jiang, Qifan Zhou,
and Xiaoji Niu^{id}, *Member, IEEE*

Abstract—Accurate and rapid INS state initialization is crucial to ensure the performance of vehicular GNSS/INS integrated navigation. However, in typical urban environments (such as under viaducts and urban canyons), existing GNSS-assisted INS state initialization methods are sensitive to observation outliers. This paper proposes a robust INS state initialization method for vehicle-mounted GNSS/INS integrated navigation. The proposed method first derives the error propagation between the short-term relative navigation (i.e., position, velocity, attitude) and the INS initial state and the GNSS observation error model; then, the high-precision relative pose generated by INS is used to construct constraints between GNSS observation sequences, and the INS state initialization problem is converted into an optimization problem; finally, a two-step optimization strategy is designed to improve the problem of high computational complexity in solving the full-state optimization problem. We use six datasets collected in a typical urban environment to verify the feasibility of the proposed method. The proposed method uses observation sequences within a 10-second to initialize the heading, velocity, and horizontal position with errors of 2.50°, 0.30 m/s, and 11.1 m, respectively, which are reduced by 73%, 41%, and 14% compared with existing methods.

Index Terms—Global navigation satellite system (GNSS)/inertial navigation system (INS) integration, navigation initialization, in-motion alignment, vehicular navigation, optimization-based alignment.

I. INTRODUCTION

INERTIAL Navigation System (INS) based on low-cost Micro-Electro-Mechanical System (MEMS) Inertial Measurement Unit (IMU) has been extensively deployed in autonomous or intelligent vehicles to achieve continuous high-frequency autonomous navigation [1], [2], [3]. However, INS has the typical characteristics of fast error accumulation

and is not suitable for long-term use alone. Therefore, INS is often used in combination with the global navigation satellite system (GNSS) in vehicle navigation to provide continuous and reliable positioning services. Since INS is a relative positioning method, its state (i.e., position, velocity and attitude) must be initially assigned when it is fused with GNSS, and the accuracy and efficiency of the initial assignment of the INS state are directly related to the robustness and effectiveness of the integrated navigation system [4].

Due to the inherent characteristics and low precision of MEMS-IMU, INS state initialization usually needs to rely on other external sensors, including GNSS [5], [6], [7], Doppler velocity log [8], [9], odometer [10], and magnetometer sensors [11]. GNSS is the most commonly used auxiliary means due to its highest penetration rate. Therefore, this paper focuses on the INS state initialization method of GNSS-assisted vehicle-mounted MEMS INS. Existing related methods can be divided into two categories: (1) Single-epoch based: These methods derive the initial position, velocity and heading from a single or double GNSS measurements. (2) Sequence based: These approaches utilize a series of GNSS observations over an extended time window (typically several seconds to minutes) to estimate the initial states. The sequence-based initialization typically employs either filtering techniques (such as Kalman filtering) or optimization algorithms.

A. Single-Epoch Based

GNSS can achieve accurate estimation of position and velocity using only single epoch observations, which is a typical initialization method based on single epoch. For attitude initialization, high-precision IMU can achieve accurate attitude acquisition by sensing gravity acceleration and earth rotation rate when stationary, while low-cost MEMS IMU has problems of large noise and large deviation, and heading initialization faces huge challenges [5]. A typical idea is to install a pair of GNSS antennas on the same vehicle to directly obtain the heading of MEMS IMU [6]. However, dual GNSS antennas will significantly increase the cost, and when the baseline length between the two GNSS antennas is too short, the GNSS heading will become very unreliable. Another idea is to determine the vehicle heading by projecting the GNSS velocity onto the horizontal plane or based on differential

Received 16 September 2024; revised 17 February 2025, 31 March 2025, and 13 May 2025; accepted 15 May 2025. This work was supported in part by the National Key Research and Development Program of China under Grant 2024YFB3909200 and in part by Hubei Provincial Natural Science Foundation Program under Grant 2023AFB021. The Associate Editor for this article was S.-H. Kong. (*Corresponding author: Yan Wang.*)

Jian Kuang, Longyang Ding, Yan Wang, and Xiaoji Niu are with the GNSS Research Center and the Hubei Technology Innovation Center for Spatiotemporal Information and Positioning Navigation, Wuhan University, Wuhan, Hubei 430072, China (e-mail: kuang@whu.edu.cn; dingly@whu.edu.cn; wystephen@whu.edu.cn; xjniu@whu.edu.cn).

Yilong Yuan, Pan Jiang, and Qifan Zhou are with the Positioning Technology Center, Tencent, Beijing 100101, China (e-mail: yosonyuan@tencent.com; mambajiang@tencent.com; qifanzhou@tencent.com).

Digital Object Identifier 10.1109/TITS.2025.3572040

positioning of adjacent GNSS positions when the vehicle is in motion [12], [13], [14]. Although the initialization method based on single epoch observation is simple and fast, it is easily affected by factors such as non-line-of-sight (NLOS) multipath effects and fails to work, and has poor robustness, especially in complex urban environments.

To mitigate the impact of GNSS gross errors on state estimation, traditional single-point GNSS quality control methods usually use the receiver autonomous integrity monitoring (RAIM) algorithm [15] to improve positioning performance. However, this method assumes that there is only one gross error in the GNSS observation, which is obviously unrealistic for challenging scenarios. Robust methods based on M-estimation attempt to reduce the impact of gross errors by modifying the shape of the cost function and using robust cost functions like Huber [16]. However, these methods fail when there are significant initial biases or a high fraction of faulty satellites in a single epoch.

B. Sequence Based

Sequence-based methods achieve INS state initialization by fusing GNSS and IMU observation sequence, include filter-based [10], [17], [18] and optimization-based [19], [20], [21]. Similarly, related research primarily focuses on the heading alignment problem. Filter-based initialization methods are usually based on a linearized or non-linear error model, and then an appropriate filter is selected to estimate the INS state. For instance, [17] investigated filter-based low-cost INS initialization methods based on the Unscented Kalman Filter (UKF), which allows for significant initial error tolerances. Reference [7] proposed a two-stage Kalman filter for achieving GPS-assisted low-cost INS heading alignment. The heading alignment error of this work can converge to 0.3° after 150 seconds of algorithm processing.

Reference [19] proposed an Optimization-Based Alignment (OBA) method, which equivalently transforms the attitude initialization problem into a continuous attitude determination problem using an infinite vector observation. Subsequently, to further enhance applicability, [22] also conducted online estimation of GNSS antenna lever arms and IMU biases based on an optimization method. While the aforementioned optimization-based initial alignment methods were initially designed for high-precision inertial navigation system, they perform well on navigation-grade IMUs. However, for low-cost MEMS IMUs, the alignment accuracy of these methods may decrease significantly when the inertial sensor biases become much larger [23]. To extend optimization-based alignment methods to low-cost MEMS IMUs, [21] proposed the Dynamic OBA algorithm, which estimates gyro biases with attitudes. Based upon the Dynamic OBA algorithm, [24] proposed a more efficient implementation. OBA methods have provided a new perspective on the alignment problem, and many follow-up studies can be found [25]. For example, [26] introduced a velocity-based optimization-based alignment method, determining attitudes based on multiple velocity vector observations and validating the method on a tractor platform. The results indicated that under low-dynamic

conditions of 1 m/s, the heading alignment error was 4° within 60 seconds.

Although the above methods offer high heading initialization accuracy, they typically require long convergence time, such as at least 50 seconds. To improve the heading initialization efficiency, [4], [14], and [27] use the displacement vector as the observation information based on the principle of trajectory similarity to realize the rapid heading initialization for MEMS IMUs. Reference [4] determines the initial heading by comparing the Real Time Kinematic (RTK) absolute trajectory and Dead Reckoning (DR) relative trajectory, and achieves an initial alignment accuracy of 0.25° in 5 seconds. Reference [27] obtain the angle by compare the actual observed Time Differenced Carrier Phase (TDCP) and INS-derived TDCP, achieving an alignment accuracy of 0.65° within 5 seconds. In general, sequence-based initialization methods require 5 to 60 seconds of sequence observations to provide high accuracy and are only applicable to open sky scenarios. However, in typical urban environments, various GNSS failures may cause filter-based or optimization-based methods to fail to converge or even diverge. In addition, carrier phase observations are very fragile and have low availability under such conditions. Therefore, the trajectory similarity-based alignment method proposed by [4] and [27] may also degenerate or even fail.

Building on the limitations of existing methods identified in the literature, current GNSS-aided MEMS INS initialization approaches exhibit two critical shortcomings: (1) degraded robustness under urban canyon environments due to reliance on single-epoch GNSS observations, and (2) limited state estimation capability focusing primarily on heading initialization. In contrast to state-of-the-art methods [4], [27], [28] that prioritize open-sky conditions, our proposed sequence-based framework introduces three key innovations:

- **Urban-Optimized robust initialization.** The proposed method takes advantage of the high relative accuracy of short-term INS and effectively “bridges” the pseudorange and Doppler observations in the sequence, making it easier to detect and eliminate observation faults through residual check, thereby achieving robust initialization of INS states.
- **Enhanced state initialization capability.** Unlike conventional approaches that estimate only heading [4], [27], our method simultaneously resolves four critical states: horizontal position (2D), vehicle velocity, heading and accelerometer biases (3D). This comprehensive initialization eliminates the need for separate calibration procedures required by prior methods.
- **Computationally efficient two-step optimization.** Aiming at the high complexity of the optimization solution, a two-step optimization strategy was designed, which significantly improved the computational efficiency of INS state estimation.

II. OVERVIEW

In a typical urban environment, due to the influence of severe signal shielding and multipath effects, GNSS single-epoch observations have serious gross errors and poor

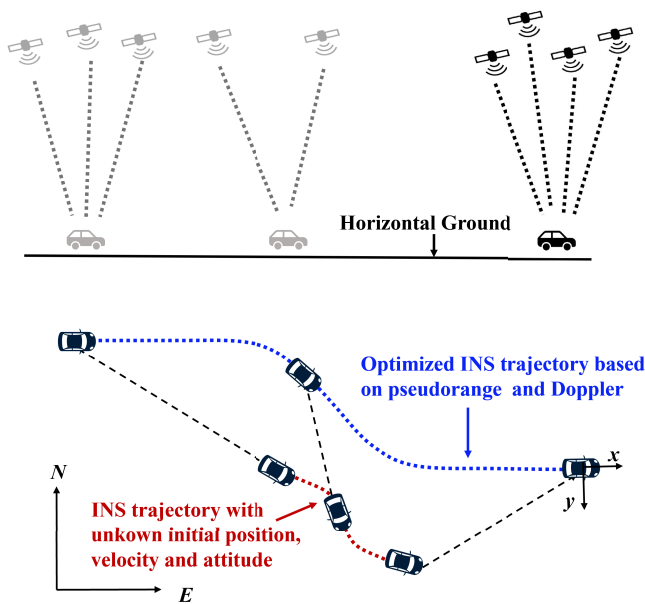


Fig. 1. Principle of the proposed initialization method.

satellite geometry. These limitations naturally motivate the adoption of sequence-based initialization approaches, which leverage continuous GNSS observations to achieve enhanced initialization accuracy through temporal integration. However, when dealing with low-cost MEMS-IMUs, the position error of INS will reach several meters in a few seconds due to their large bias instabilities and high noise. This rapid error growth undermines the reliability of the relative position and attitude relationships that are crucial for effective sequence-based initialization. Consequently, the development of robust sequence-based initialization methods must address both the GNSS fault observation issues in urban environments and the inherent limitations of low-cost MEMS-IMUs.

This paper assumes that the errors of short-term INS position and velocity are completely attributed to the navigation state error of the first epoch of the observation sequence, and uses relative position and velocity to construct the association of multi-epoch GNSS pseudorange and Doppler. Finally, the robust initialization of INS state is achieved by simultaneously optimizing INS state errors and detecting GNSS observation gross errors. Essentially, the vehicle dynamics obtained by the two observation methods should be objectively consistent. INS provides continuous relative position, velocity and attitude, while GNSS provides discrete absolute position and velocity.

Figure 1 illustrates the basic principle of the proposed INS state initialization method. The INS state initialization process can be intuitively understood as translating, scaling, and rotating the trajectory and velocity obtained by the INS in order to achieve consistency with the GNSS pseudorange and Doppler. Among them, translation corresponds to position initialization, scaling corresponds to velocity initialization and accelerometer bias estimation, and rotation corresponds to heading initialization.

TABLE I
DESCRIPTION AND DEFINITIONS OF THE COORDINATE SYSTEMS

Symbol	Description	Definition
v -frame	The vehicle frame.	origin: the center of mass of the vehicle. x -axis: pointing to the vehicle's forward direction. y -axis: pointing to the right of the vehicle. z -axis: completing a right-handed orthogonal frame.
n -frame	The navigation frame (i.e., the local north-east-down frame).	origin: the same as b -frame. x -axis: towards geodetic north. z -axis: orthogonal to the reference ellipsoid pointing down. y -axis: completing a right-handed orthogonal frame.
b -frame	The body frame (i.e., the coordinate system of the IMU).	origin: IMU measurement center. x -axis, y -axis and z -axis: the IMU's body axes.

III. THE PROPOSED METHOD

Before describing the proposed method in detail, the following assumptions should be clarified:

Assumption 1: We assume that the mounting angle between the IMU frame and the vehicle frame is known and can be accurately determined using the method described in [29].

Assumption 2: We assume that the horizontal angles (i.e. roll and pitch) are known. This assumption is reasonable because the horizontal angles can be obtained using an Attitude and Heading Reference System (AHRS) [30], [31]. Importantly, the AHRS in our framework relies only on accelerometer and gyroscope data for horizontal angles estimation, eliminating the need for external sensors (e.g., magnetometers) and ensuring immunity to GNSS measurement outliers.

The definitions of the main coordinate systems involved in this paper are listed in Table I.

A. System State Definition

The system states to be estimated in the initialization problem of this paper can be represented as:

$$\begin{cases} \boldsymbol{\chi} &= [\boldsymbol{x}_{ins} \ \boldsymbol{x}_{gnss}] \\ \boldsymbol{x}_{ins} &= [\boldsymbol{p}_0^n \ v_{f,0}^v \ \psi_0 \ \boldsymbol{b}_{a,0}] \\ \boldsymbol{x}_{gnss} &= [t_{bias,0}^G \ t_{drift,0}^C] \end{cases} \quad (1)$$

where \boldsymbol{x}_{ins} and \boldsymbol{x}_{gnss} represent the INS-related and GNSS-related state vector, respectively; \boldsymbol{p}_0^n represents the initial position vector in the n -frame; $v_{f,0}^v$ represents the initial forward velocity in the v -frame; ψ_0 represents the initial heading; $\boldsymbol{b}_{a,0}$ represents the initial accelerometer bias; $\boldsymbol{t}_{bias,0} = [t_{bias,0}^G \ t_{bias,0}^C]$ represents the receiver clock bias vector, include GPS and BDS satellite systems; $t_{drift,0}$ represents the receiver clock drift; the right subscript "0" represents the first epoch of the sequence.

In addition, low-cost MEMS IMUs usually have large initial gyroscope bias and accelerometer bias. Gyroscope bias directly affects the accuracy of attitude estimation,

and accelerometer bias directly reduces the accuracy of velocity estimation. Therefore, for sequence-based INS initialization methods, such errors should be eliminated or estimated as much as possible. For large gyroscope bias, it is usually eliminated by subtracting the average value of gyroscope observations in the stationary state of the carrier in practical applications, while the residual gyroscope bias has little effect on the fast initialization method [4]. However, the accelerometer bias does not have similar conditions, and its impact on velocity estimation is significant. Thus, this paper includes the initial accelerometer bias $\mathbf{b}_{a,0}$ as an unknown state parameter to improve the accuracy of the initialization process.

B. INS Error Modeling

Due to the poor performance of low-cost MEMS IMUs, ignoring small error correction terms such as the earth's rotation usually does not lead to significant performance differences [32], so this paper adopts a simplified inertial navigation algorithm as follows:

$$\begin{cases} \mathbf{p}_k &= \mathbf{p}_{k-1} + \mathbf{D}_r^{-1} \mathbf{v}_k^n \Delta t_k \\ \mathbf{v}_k^n &= \mathbf{v}_{k-1}^n + \mathbf{C}_{b,k}^n \Delta \mathbf{v}_k^b + \mathbf{g}^n \Delta t_k \\ \mathbf{C}_{b,k}^n &= \mathbf{C}_{b,k-1}^n [\mathbf{I} + \Delta \boldsymbol{\theta}_k^b \times] \end{cases} \quad (2)$$

where $\mathbf{p} = [\varphi \ \lambda \ h]^T$ represents the curvilinear position vector, where the three components denote latitude, longitude and height, respectively; $\mathbf{v}^n = [v_N \ v_E \ v_D]^T$ represents the velocity vector in the n -frame, where the three components denote north, east and down velocity, respectively; $\mathbf{D}_r = \text{diag}([R_m + h \ (R_n + h) \cos \varphi \ -1]^T)$, where R_m is the radius of curvature in the meridian and R_n is the radius of curvature in the prime vertical; \mathbf{C}_b^n represents the direction cosine matrix from the b -frame to the n -frame; $\mathbf{g}^n = [0 \ 0 \ -9.8]^T$ is Earth's gravity vector; $\Delta \mathbf{v}_k^b = (\tilde{\mathbf{f}}_k^b - \mathbf{b}_{a,k}) \Delta t_k$ is the velocity increment in the b -frame; $\tilde{\mathbf{f}}^b$ and \mathbf{b}_a are the acceleration and bias of the accelerometer, respectively; $\Delta \boldsymbol{\theta}_k^b = (\tilde{\boldsymbol{\omega}}_k^b - \mathbf{b}_{\omega,k}) \Delta t_k$ is the angle increment in the b -frame; $\tilde{\boldsymbol{\omega}}^b$ and \mathbf{b}_g are the angle rate and bias of the gyroscope, respectively; $\Delta t_k = t_k - t_{k-1}$ is the time interval between the $(k-1)$ -th and k -th epoch; and \times is the cross-product form of a vector.

Although the errors of INS based on low-cost MEMS IMUs accumulate rapidly over time, the short-term relative accuracy is still reliable [33]. Based on Eq. 2, this paper models the INS state error within a short time window as a variable that only depends on the initial INS state error and the accelerometer bias error. Next, we derive the attitude, velocity, and position at time t_k as a function of the initial state \mathbf{x}_{ins} .

1) *Attitude*: Based on the chain rule of rotation matrices, the estimated attitude at time t_k can be expressed as:

$$\hat{\mathbf{C}}_{b,k}^{n,k} = \hat{\mathbf{C}}_{n,0}^{n,k} \hat{\mathbf{C}}_{b,0}^{n,0} \hat{\mathbf{C}}_{b,k}^{b,0} \quad (3)$$

where the notation $\hat{\cdot}$ denotes an unknown or computed variable; $\hat{\mathbf{C}}_{b,k}^{n,k}$ represents the computed attitude matrix at epoch k ; $\hat{\mathbf{C}}_{n,0}^{n,k}$ represents the change of the n -frame from epoch 0 to epoch k , which accounts for the rotation of the n -frame due

to the movement of the vehicle; $\hat{\mathbf{C}}_{b,0}^{n,0}$ represents the initial attitude matrix to be determined during alignment at epoch 0. $\hat{\mathbf{C}}_{b,k}^{b,0} = (\hat{\mathbf{C}}_{b,0}^{b,k})^T$, $\hat{\mathbf{C}}_{b,0}^{b,k}$ represents the integral result of the gyroscope measurements from epoch 0 to epoch k using Eq. 2. Then, we made the following approximations:

Approximation 1: $\mathbf{C}_{n,0}^{n,k} \approx \mathbf{I}$. The rationale for this approximation lies in the fact that the rotation of the n -frame due to vehicle motion can be considered negligible over a short time interval (e.g., less than 30 seconds).

Approximation 2: $\hat{\mathbf{C}}_{b,k}^{b,0} \approx \mathbf{C}_{b,k}^{b,0}$. This approximation is justified because the error in $\hat{\mathbf{C}}_{b,k}^{b,0}$ primarily arises from gyroscope measurement errors, including residual bias, scale factor error, non-orthogonality error, and random noise. During the initial alignment period, the error in $\hat{\mathbf{C}}_{b,k}^{b,0}$ is significantly smaller than the heading error in $\hat{\mathbf{C}}_{b,0}^{n,0}$ [4]. Eq. 3 can be rewritten as:

$$\hat{\mathbf{C}}_{b,k}^{n,k} = \hat{\mathbf{C}}_{b,0}^{n,0} \mathbf{C}_{b,k}^{b,0} \quad (4)$$

Then the errors contained in the computed matrix $\hat{\mathbf{C}}_{b,k}^{n,k}$ only come from the error in $\hat{\mathbf{C}}_{b,0}^{n,0}$. According to Assumption 2, the roll and pitch angles could be determined by AHRS with an error notably smaller than the initial heading. Therefore, it's reasonable to assume that the only unknown parameter in $\hat{\mathbf{C}}_{b,0}^{n,0}$ is the heading angle.

2) *Velocity*: Similarly, the velocity at time t_k computed by integrating the accelerometer observations can be expressed as:

$$\begin{aligned} \hat{\mathbf{v}}_k^n &= \hat{\mathbf{v}}_0^n + \sum_{j=1}^k \hat{\mathbf{C}}_{b,j}^{n,j} \Delta \hat{\mathbf{v}}_j^b - \sum_{j=1}^k \mathbf{g}^n \Delta t_j \\ &= \hat{\mathbf{C}}_{b,0}^{n,0} \mathbf{C}_v^b \hat{\mathbf{v}}_0^v + \sum_{j=1}^k \hat{\mathbf{C}}_{b,0}^{n,0} \mathbf{C}_{b,j}^{b,0} (\tilde{\mathbf{f}}_j^b - \hat{\mathbf{b}}_{a,0}) \Delta t_j - \sum_{j=1}^k \mathbf{g}^n \Delta t_j \\ &= \hat{\mathbf{C}}_{b,0}^{n,0} \mathbf{C}_v^b \hat{\mathbf{v}}_0^v + \sum_{j=1}^k \hat{\mathbf{C}}_{b,0}^{n,0} \mathbf{C}_{b,j}^{b,0} \tilde{\mathbf{f}}_j^b \Delta t_j \\ &\quad - \sum_{j=1}^k \hat{\mathbf{C}}_{b,0}^{n,0} \mathbf{C}_{b,j}^{b,0} \hat{\mathbf{b}}_{a,0} \Delta t_j - \sum_{j=1}^k \mathbf{g}^n \Delta t_j \end{aligned} \quad (5)$$

where $\mathbf{C}_v^v = (\mathbf{C}_v^b)^T$ represents the direction cosine matrix from the b -frame to the v -frame, which is a known parameter according to Assumption 1; $\hat{\mathbf{v}}_0^v = [\hat{v}_{fw,0}^v \ 0 \ 0]$ represents the velocity vector in the v -frame, $\hat{v}_{fw,0}^v$ represents the initial forward speed of the vehicle. This paper assumes that the vehicle meets the non-holonomic constraints that the lateral and vertical velocities are zero; $\hat{\mathbf{b}}_{a,0}$ represents the accelerometer bias over a short time window is modeled as a constant. The computed velocity $\hat{\mathbf{v}}_k^n$ at time t_k is mainly affected by $\hat{\mathbf{C}}_{b,0}^{n,0}$, $\hat{\mathbf{v}}_0^v$, and $\hat{\mathbf{b}}_{a,0}$.

3) *Position*: The position at time t_k can be computed by integrating the velocity:

$$\hat{\mathbf{p}}_k^n = \hat{\mathbf{p}}_0^n + \sum_{i=1}^k \hat{\mathbf{v}}_i^n \Delta t_i \quad (6)$$

Substituting Eq. 5 into Eq. 6, we have:

$$\begin{aligned} \hat{\mathbf{p}}_k^n &= \hat{\mathbf{p}}_0^n + \sum_{i=1}^k \left(\hat{\mathbf{C}}_{b,0}^{n,0} \mathbf{C}_{b,0}^{b,0} \hat{\mathbf{v}}_0^v \right) \Delta t_i \\ &+ \sum_{i=1}^k \left(\sum_{j=1}^i \hat{\mathbf{C}}_{b,0}^{n,0} \mathbf{C}_{b,j}^{b,0} \tilde{\mathbf{f}}_j^b \Delta t_j \right) \Delta t_i \\ &- \sum_{i=1}^k \left(\sum_{j=1}^i \hat{\mathbf{C}}_{b,0}^{n,0} \mathbf{C}_{b,j}^{b,0} \hat{\mathbf{b}}_{a,0} \Delta t_j \right) \Delta t_i \\ &- \sum_{i=1}^k \left(\sum_{j=1}^i \mathbf{g}^n \Delta t_j \right) \Delta t_i \end{aligned} \quad (7)$$

The computed position $\hat{\mathbf{p}}_k^n$ at time t_k is influenced by $\hat{\mathbf{p}}_0^n$, $\hat{\mathbf{C}}_{b,0}^{n,0}$, $\hat{\mathbf{v}}_0^v$, and $\hat{\mathbf{b}}_{a,0}$.

C. INS Error Propagation Analysis

The previous section established the functional relationship between the INS-derived states (attitude, velocity, and position) at time t_k and the initial state \mathbf{x}_{ins} , while intentionally omitting the effects of residual gyroscope biases and random measurement noise. To justify this modeling approach, we now present a comprehensive error analysis focusing on the dominant IMU error sources that influence short-term INS performance.

The IMU measurements errors include random noise, biases, and scale factor errors. Given that random noise and scale factor effects are negligible over short time-spans [4], our analysis concentrates on bias-induced errors. The gyroscope bias \mathbf{b}_g directly contaminates attitude estimation, subsequently affecting the specific force projection in the navigation frame. Following the derivation in [13], under constant-velocity motion assumptions, the residual gyroscope bias-induced errors propagate as:

$$\begin{cases} \delta \boldsymbol{\psi} \approx \mathbf{b}_g t \\ \delta \mathbf{v}^n \approx \frac{1}{2} \mathbf{C}_b^n (\mathbf{b}_g \times \mathbf{g}^n) t^2 \\ \delta \mathbf{r}^n \approx \frac{1}{6} \mathbf{C}_b^n (\mathbf{b}_g \times \mathbf{g}^n) t^3 \end{cases} \quad (8)$$

where $\boldsymbol{\psi}$, $\delta \mathbf{v}^n$, $\delta \mathbf{r}^n$ denotes attitude error, velocity error and position error, respectively. Considering that the dominant constant bias can be pre-calibrated through static periods, the residual gyro bias (including Earth rotation rate) is typically bounded below 18 deg/h [14]. For a 10-seconds initialization window, this yields: $\delta \boldsymbol{\psi} \approx 0.05^\circ$, $\delta \mathbf{v}^n \approx 0.043$ m/s, $\delta \mathbf{r}^n \approx 0.143$ m. These errors remain negligible compared to typical state initialization errors, justifying our exclusion of residual gyro bias in the state vector.

Given that velocity is obtained through the integration of acceleration and position is derived from the integration of velocity, the impact of accelerometer biases \mathbf{b}_a on velocity and position errors can be expressed as:

$$\begin{cases} \delta \mathbf{v}^n \approx \mathbf{C}_b^n \mathbf{b}_a t \\ \delta \mathbf{r}^n \approx \frac{1}{2} \mathbf{C}_b^n \mathbf{b}_a t^2 \end{cases} \quad (9)$$

For low-cost MEMS accelerometers with typical bias instability of 0.05 m/s², the 10-seconds error accumulation becomes: $\delta \mathbf{v}^n \approx 0.5$ m/s, $\delta \mathbf{r}^n \approx 2.5$ m. This non-negligible error necessitates explicit modeling of accelerometer biases in our optimization problem. Therefore, we include \mathbf{b}_a as estimated parameters to improve initialization accuracy.

D. Pseudorange and Doppler

In complex urban environments, the GNSS/INS tight combination can use GNSS raw observations, and the positioning performance in some sky-blocked areas is better than that of the GNSS/INS loose combination. To this end, this paper uses GNSS raw observations to initialize the INS state to ensure efficiency and robustness. Due to the low fragility and availability of carrier phase observations in complex environments, this study only uses pseudorange and Doppler observations. Pseudorange observations can be expressed as:

$$\tilde{\rho}_k^{s_j} = \rho_k^{s_j} + c \left(t_{bias,k}^{s_j} - t_{bias,k} \right) + I_k^{s_j} + T_k^{s_j} + M_k^{s_j} + \varepsilon_\rho^{s_j} \quad (10)$$

where the subscript k represents the epoch number and the superscript s_j represents the j -th satellite; $\rho_k^{s_j}$ represents the geometric distance between the GNSS receiver and the satellite; c represents the speed of light; $t_{bias,k}^{s_j}$ represents the satellite clock bias, which can be obtained from ephemeris; $t_{bias,k}$ represents the receiver clock bias; $I_k^{s_j}$ and $T_k^{s_j}$ represent the ionospheric and tropospheric delays, respectively, atmospheric errors are modeled and subtracted following the methods in RTKLIB [34]; $M_k^{s_j}$ represents the multipath effect; $\varepsilon_\rho^{s_j}$ represents the measurement noise, assumed to follow a zero-mean Gaussian distribution, such that $\varepsilon_\rho^{s_j} \sim N(0, (\sigma_\rho^{s_j})^2)$. The standard deviation of $\sigma_\rho^{s_j}$ of $\varepsilon_\rho^{s_j}$ is modeled as an elevation angle model:

$$\sigma_\rho^{s_j} = \sqrt{\frac{\sigma_\rho^2}{\sin^2(e l_k^{s_j})}} \quad (11)$$

Here σ_ρ is the priori zenith pseudorange measurement standard deviation, and $e l_k^{s_j}$ signifies the satellite elevation angle as seen from the receiver at epoch t_k . Ignoring the lever arm between the GNSS antenna and the IMU, single pseudorange residual can be expressed as:

$$\left\| \mathbf{e}_{k,\rho}^{s_j} \right\|_{\sigma_{k,\rho}^{s_j}}^2 = \left\| \tilde{\rho}_k^{s_j} - \mathbf{h}_{\rho,k}^{s_j}(\mathbf{x}_{ins}, t_{bias,k}) \right\|_{\sigma_{k,\rho}^{s_j}}^2 \quad (12)$$

$$\mathbf{h}_{\rho,k}^{s_j}(\mathbf{x}_{ins}, t_{bias,k}) = \left\| \mathbf{p}_k^{s_j} - \hat{\mathbf{p}}_{ins,k} \right\| + c \cdot t_{bias,k} \quad (13)$$

where $\hat{\mathbf{p}}_{ins,k}$ is the position predicted by INS and $\mathbf{p}_k^{s_j}$ is the satellite position. Doppler are modeled as:

$$\tilde{D}_k^{s_j} = -\frac{1}{\lambda} \left[\mathbf{E}_k^{s_j} (\mathbf{v}_k^{s_j} - \mathbf{v}_k) + c \left(t_{drift,k} - t_{drift,k}^s \right) \right] + \varepsilon_D^{s_j} \quad (14)$$

where λ represents the carrier wavelength; $\mathbf{v}_k^{s_j}$ and \mathbf{v}_k represent the satellite and receiver velocity vectors, respectively; $\mathbf{E}_k^{s_j}$ represents the line-of-sight (LOS) unit vector from the receiver to the satellite; $t_{drift,k}^s$ is the satellite clock drift,

reported in the navigation message; $\varepsilon_D^{s_j}$ represents the Doppler measurement noise, assumed to follow a zero-mean Gaussian distribution, such that $\varepsilon_D^{s_j} \sim N(0, (\sigma_D^{s_j})^2)$. The standard deviation of $\sigma_D^{s_j}$ of $\varepsilon_D^{s_j}$ is modeled as:

$$\sigma_D^{s_j} = \sqrt{\frac{\sigma_D^2}{\sin^2(\varepsilon_k^{s_j})}} \quad (15)$$

Here σ_D is the priori zenith Doppler measurement standard deviation. Then, the Doppler measurement residual at epoch t_k can be formulated as:

$$\|\mathbf{e}_{k,D}^{s_j}\|_{\sigma_{k,D}^{s_j}}^2 = \|\tilde{D}_k^{s_j} - \mathbf{h}_{D,k}^{s_j}(\mathbf{x}_{ins}, t_{drift,k})\|_{\sigma_{k,D}^{s_j}}^2 \quad (16)$$

$$\mathbf{h}_{D,k}^{s_j}(\mathbf{x}_{ins}, t_{drift,k}) = -\frac{1}{\lambda} \left[\mathbf{E}_k^{s_j} (\mathbf{v}_k^{s_j} - \hat{\mathbf{v}}_{ins,k}) + c \cdot t_{drift,k} \right] \quad (17)$$

where $t_{drift,k}$ denotes the receiver clock drift at epoch k , which can be modeled as constant over short periods. The receiver clock bias at epoch k (i.e., $t_{bias,k}$) can be modeled using the clock drift model:

$$\begin{cases} t_{drift,k} &= t_{drift,0} \\ t_{bias,k} &= t_{bias,0} + t_{drift,0} (t_k - t_0) \end{cases} \quad (18)$$

E. Two-Step Optimization Algorithm

Based on the INS error model, pseudorange and Doppler observation model, the INS state initialization problem can be transformed into a state estimation problem, and accurate state estimation can be achieved by solving the following optimization problem:

$$\chi = \arg \min_{\chi} \sum_{k=1}^N \sum_{j=1}^{S_k} \left(\|\mathbf{e}_{k,D}^{s_j}\|_{\sigma_{k,D}^{s_j}}^2 + \|\mathbf{e}_{k,\rho}^{s_j}\|_{\sigma_{k,\rho}^{s_j}}^2 \right) \quad (19)$$

where N denotes the length of the observation sequence; S_k represents the number of satellites at epoch t_k . The Gauss-Newton method [35] was used to solve the above optimization problem. However, in complex urban environments, satellite signals are susceptible to multipath and non-line-of-sight signals, and there are significant errors in pseudorange and Doppler observations, which leads to the challenge of optimization failing to converge to the global minimum. To this end, the Huber robust kernel function [16] is used to reduce the impact of pseudorange and Doppler gross errors on the accuracy of nonlinear optimization. The optimization problem can be further expressed as:

$$\chi = \arg \min_{\chi} \sum_{k=1}^N \sum_{j=1}^{S_k} \Theta \left(\|\mathbf{e}_{k,D}^{s_j}\|_{\sigma_{k,D}^{s_j}}^2 + \|\mathbf{e}_{k,\rho}^{s_j}\|_{\sigma_{k,\rho}^{s_j}}^2 \right) \quad (20)$$

where the Huber norm is defined as:

$$\Theta(s) = \begin{cases} s, & s \leq 1 \\ 2\sqrt{s} - 1, & s > 1. \end{cases} \quad (21)$$

Due to the characteristics of the GNSS signal structure, Doppler are typically an order of magnitude more accurate than pseudorange [36], we design a two-step optimization

method to achieve more robust and efficient state estimation. Specifically, we first solve the initial velocity, heading, accelerometer bias, and clock drift based on Doppler; then, we solve the initial position and clock bias based on pseudorange. Let:

$$\chi_1 = [\mathbf{v}_{fw,0}^v \ \psi_0 \ \mathbf{b}_{a,0} \ t_{drift,0}] \quad (22)$$

$$\chi_2 = [\mathbf{p}_0^n \ t_{bias,0}] \quad (23)$$

Thus, to solve the initialization problem, the first step is:

$$\chi_1 = \arg \min_{\chi} \sum_{k=1}^N \sum_{j=1}^{S_k} \Theta \left(\|\mathbf{e}_{k,D}^{s_j}\|_{\sigma_{k,D}^{s_j}}^2 \right) \quad (24)$$

and the second step is:

$$\chi_2 = \arg \min_{\chi} \sum_{k=1}^N \sum_{j=1}^{S_k} \Theta \left(\|\mathbf{e}_{k,\rho}^{s_j}\|_{\sigma_{k,\rho}^{s_j}}^2 \right) \quad (25)$$

Since the state estimation process is non-linear with respect to some of the system states, its performance is affected by the initial values. In this paper, the initial values of position and velocity are obtained through SPP with the Huber robust cost function, while the initial values of clock bias and clock drift are directly set to zero due to their linearity. The initial heading is obtained by averaging the compensated gyro-integrated heading from multiple GNSS velocity headings as follows:

$$\psi_{0,init} = \frac{1}{N} \sum_{k=1}^N (\psi_{k,gnss} - \Delta\psi_{0,k}) \quad (26)$$

where $\psi_{0,init}$ represents the calculated initial heading at epoch 0; $\psi_{k,gnss}$ denotes the heading at epoch k derived from GNSS velocity measurements; $\Delta\psi_{0,k}$ represents the INS-derived heading change from epoch 0 to epoch k . The averaging over k epochs reduce the impact of noise and improve the accuracy of the initial heading. The implementation process of the proposed method is presented in Algorithm 1.

IV. EXPERIMENTS AND RESULTS

A. Experiments Description

To evaluate the performance of the proposed INS state initialization method, multiple vehicle road test experiments were conducted in a typical GNSS challenge environment in Wuhan. Figure 2 shows the installation structure of the equipment used in the experiment. INS-Probe is a test device used to evaluate the performance of the proposed method. It is a GNSS/MEMS-IMU integrated module independently developed by our project team, integrating MEMS IMU ICM20602 and ublox F9P, and has millimeter-level time synchronization capability. ICM20602 provides IMU data with a sampling rate of 200 Hz; ublox F9P supplies single-frequency BDS/GPS pseudorange and Doppler observations with a data rate of 1 Hz. The main parameters of ICM20602 are listed in Table II. The ground truth equipment includes a navigation-grade IMU (LD-A15, Lide Space Information Technology Co., Ltd., China), a professional GNSS receiver (Panda, Panda Space-Time Technology Co., Ltd., China) and

Algorithm 1 Proposed INS Navigation State Initialization Method

Require:

- IMU data sequence;
- Pseudorange measurements sequence;
- Doppler sequence;

Ensure:

INS position, velocity and heading at current time;

- 1: Determine initial values of INS states;
- 2: Calculate attitude, velocity, and position sequences by integrating IMU measurements using Eq. 2;
- 3: Construct Doppler observation residuals Eq. 24;
- 4: Solve Eq. 24 using the Gauss-Newton method until convergence or the preset maximum number of iterations is reached;
- 5: **if** Eq. 24 converges **then**
- 6: Construct pseudorange observation residuals Eq. 25;
- 7: Solve Eq. 25 using the Gauss-Newton method until convergence or the preset maximum number of iterations is reached;
- 8: **if** Eq. 25 converges **then**
- 9: Calculate INS position, velocity and heading at current time.
- 10: **end if**
- 11: **end if**



Fig. 2. Experiment platforms.

a high-precision wheel odometer. The ground truth is achieved by a smoothed PPK/INS/odometer integration method, achieving position accuracy better than 1m, attitude accuracy better than 0.01 degrees, and velocity accuracy better than 5cm/s. Equipment not marked in the figure is not related to this study.

Figure 3 shows the trajectories and locations of the three routes used in the vehicle experiments, passing through various GNSS-vulnerable scenarios such as alleys, urban canyons, and under overpasses. The dataset covers three complex urban routes, with two sets of data collected for each route. The two sets for Route A were independently collected, while the datasets for Routes B and C were collected simultaneously using two INS-Probe units in a single test. The total duration of

TABLE II
PERFORMANCE PARAMETERS OF ICM20602

Performance	
Gyroscope bias (deg/h)	50
Angular random walk (deg/\sqrt{h})	0.24
Accelerometer bias ($mGal$)	500
Velocity random walk ($m/s/\sqrt{h}$)	0.24

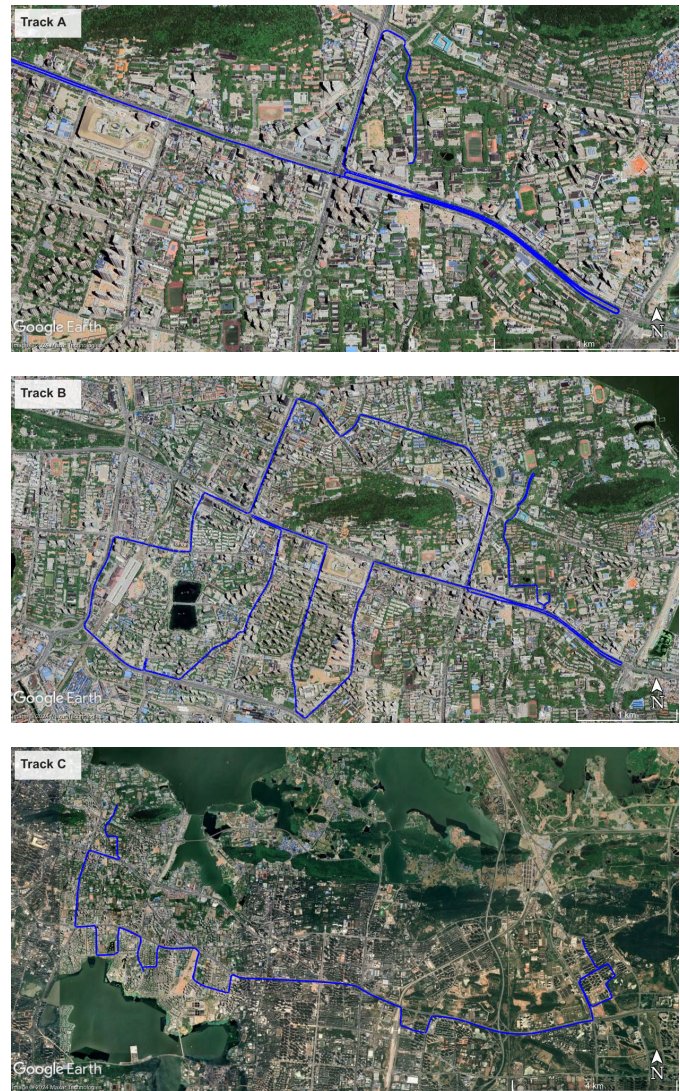


Fig. 3. Experimental trajectories (from Google Earth).

TABLE III
VEHICLE MOTION INFORMATION IN THE EXPERIMENTS

Dataset	Track	Average speed (km/h)	Data length (h)
A1	A	26.7	1.20
A2	A	21.1	0.94
B1	B	16.9	1.39
B2	B	16.9	1.39
C1	C	17.8	1.59
C2	C	17.8	1.59

the data is approximately 8 hours. Table III provides detailed motion information for each dataset.

B. Data Processing

After the vehicle road test data is collected, the GNSS raw observations (single-frequency BDS/GPS pseudorange + Doppler) and IMU data are divided into small segments (e.g., 10 seconds per segment) to simulate the working conditions of INS state initialization in real application scenarios. The segment length is set to 10 seconds as a result of comprehensive consideration of the efficiency and accuracy of INS state initialization. For more details on the impact of segment length on the accuracy of INS state initialization, see section IV-D.3. It is worth noting that although we use post-processing to perform performance evaluation, the proposed method can also be performed under real-time navigation working conditions. The specific process of data processing is as follows:

- 1) **Low-speed Data Exclusion:** Since the initial heading of the proposed method becomes unobservable when the vehicle speed is zero, only data corresponding to vehicle speeds exceeding 1 m/s are considered in the performance evaluation of the method.
- 2) **Sample Extraction:** 10 seconds of continuous IMU observations and GNSS pseudorange and Doppler data are used as 1 sample for INS state initialization.
- 3) **Algorithm Execution:** The proposed algorithm is executed using the data samples generated in step 2 as input.
- 4) **Error Calculation:** The output of the proposed algorithm is compared with the reference value, and the difference is the heading error, velocity error, and position error of one sample.
- 5) Repeat steps 1-4 until all samples in the dataset have been processed.

To verify the effectiveness of the proposed method and evaluate the accuracy of INS state initialization, we compared the following methods:

- **RTKLIB [34]:** A widely used single epoch based initialization method. RTKLIB uses a simple RAIM algorithm and chi-square test for GNSS quality control, and the SPP solution directly provides the initial position and velocity. At the same time, the arc tangent of the estimated GNSS velocity is used to calculate the initial heading.
- **OB-SPP:** Improved single-epoch initialization method. To mitigate the impact of pseudorange and Doppler gross errors, the Huber robust kernel function is used to improve the position and velocity estimation accuracy of the SPP scheme. Similarly, the initial heading is obtained by taking the arc tangent of the velocity.
- **Chen [4]:** A sequence-based heading initialization method proposed by our team in previous work. The principle of this method is as follows: The relative trajectory of the vehicle is calculated by using the MEMS-gyro observations to estimate the attitude of the vehicle and the travel distance provided by GNSS. The initial heading is then calculated by comparing DR-indicated with GNSS-indicated trajectories. The GNSS position provided by the RTKLIB solution was used as input to this method for heading initialization.

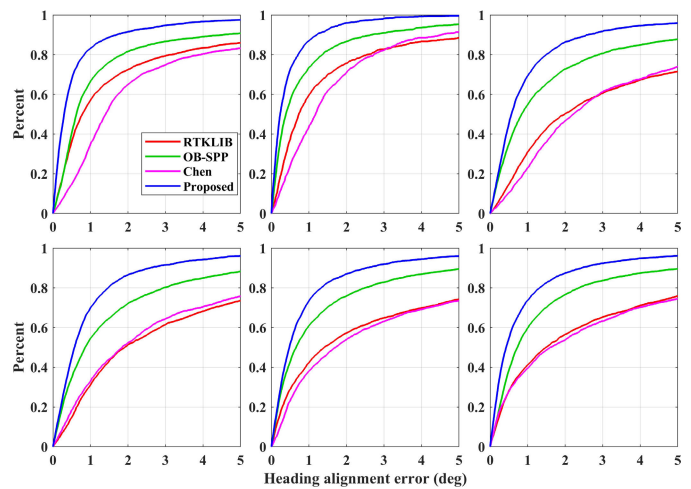


Fig. 4. CDF of heading error for RTKLIB, OB-SPP, Chen, and the proposed method using six datasets.

- **Proposed:** The INS state initialization method proposed in this paper.

C. INS State Initialization Error

We evaluate the proposed method using six datasets collected in urban complex environments and compare it with RTKLIB, OB-SPP, and Chen methods. Among them, Chen is an INS heading initialization method, and the relevant comparative analysis is only performed on the heading error part.

1) **Heading Error:** Fig. 4 shows the Cumulative Density Function (CDF) of the heading error for the four methods using six datasets. Root Mean Square (RMS) of heading error for the four methods using six datasets are shown in Table IV. The average heading error for RTKLIB, OB-SPP, and Chen are 10.57° , 9.43° , and 11.47° , respectively. The heading errors for the proposed method using six datasets ranges from 0.95° to 3.23° , and the average heading error is 2.50° . Compared with the existing methods, the proposed method reduces the heading error by 76%, 73%, and 78% respectively, achieving robust heading initialization at the degree level.

In complex urban environment, multipath effect and NLOS can cause a large number of GNSS pseudorange and Doppler observation gross errors, and the heading initialization scheme based on RTKLIB uses RAIM algorithm to deal with this phenomenon. Moreover, RTKLIB assumes that there is only one observation error, which is seriously inconsistent with the actual situation, resulting in low accuracy of heading initialization. To address this problem, OB-SPP uses the Huber robust kernel function to reduce the impact of the error, releasing the assumption that there is only one error in GNSS observations, so that a higher-precision initialization heading can be obtained. In Table IV, the heading error of OB-SPP relative to RTKLIB is only reduced from 10.57° to 9.43° . This is because RTKLIB performs a chi-square test on some areas with severe errors and excludes some errors from the final statistical results. In fact, OB-SPP has a more obvious improvement in initial heading accuracy relative to RTKLIB. Nevertheless, when the proportion of faulty satellite observations in an epoch is high, the heading initialization

TABLE IV
RMS OF HEADING ERROR FOR RTKLIB, OB-SPP, CHEN, AND THE PROPOSED METHOD USING SIX DATASETS (UNIT: °)

Dataset	RTKLIB			OB-SPP			Chen			Proposed		
	RMS	68%	95%	RMS	68%	95%	RMS	68%	95%	RMS	68%	95%
A1	9.03	1.60	13.53	8.93	1.06	9.33	16.93	2.22	21.00	1.80	0.50	3.11
A2	10.12	1.39	10.40	10.92	0.80	4.82	6.19	1.85	9.31	0.95	0.43	1.81
B1	11.70	4.11	20.38	9.22	1.67	12.44	14.21	4.04	20.24	3.23	0.96	4.22
B2	11.22	3.92	20.06	10.87	1.69	11.86	10.33	3.37	19.81	3.15	0.94	4.34
C1	11.59	3.62	20.59	8.21	1.37	10.84	11.76	3.72	21.91	3.07	0.83	4.27
C2	9.75	3.51	18.62	8.41	1.37	9.52	9.39	3.63	20.89	2.79	0.81	4.12
Average	10.57	3.03	17.26	9.43	1.32	9.80	11.47	3.14	18.86	2.50	0.74	3.64

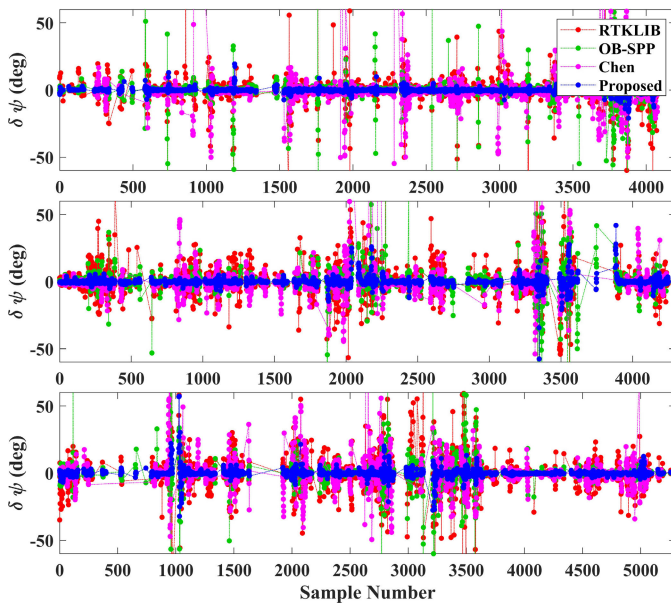


Fig. 5. Heading error for RTKLIB, OB-SPP, Chen, and the proposed method using dataset A1, B1 and C1.

accuracy of OB-SPP will still drop sharply. Compared with the single-epoch based initialization method, the proposed method cleverly utilizes more GNSS observations with the help of the high-precision relative pose of INS, dilutes the proportion of faulty satellites, makes gross errors easier to identify, and has better robustness.

Our previous work (Chen [4]) achieved the heading initialization accuracy of 4.7° with 98.6% confidence in 5-second sequence length in SPP mode. However, the results from this study show that the average heading error of this method is only 11.47° , which seems lower than expected. This discrepancy is mainly due to differences in the datasets: the datasets in this study were primarily collected in complex urban environments, where significant GNSS gross errors lead to large SPP position errors, greatly affecting the heading initialization accuracy. Additionally, the datasets were collected on an urban road with relatively heavy traffic, and the average vehicle speed was lower than the average speed of 15 m/s in [4], which would result in higher noise in the heading estimation.

Fig. 5 shows the heading error for the four initialization methods using dataset A1, B1 and C1. The proposed method significantly outperforms all the other comparison

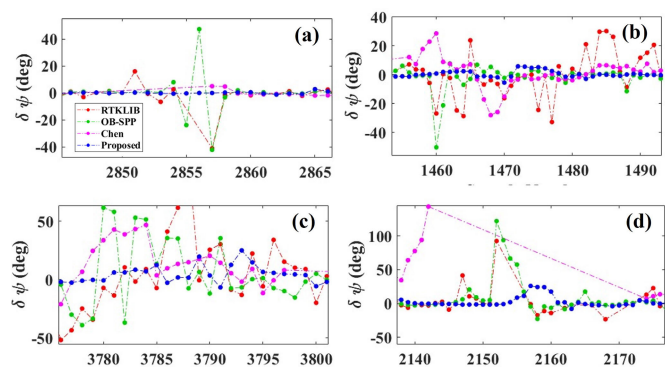


Fig. 6. Heading error for RTKLIB, OB-SPP, Chen, and the proposed method at different time periods.

methods and shows excellent robustness in challenging urban environment. For further illustration, we select several road sections from Fig. 5. Figure 6 (a) shows the heading error corresponding to a short passage under an overpass. The chi-square test in RTKLIB eliminated some samples with serious gross errors, which resulted in the Chen method being unable to complete heading initialization normally due to the lack of available GNSS positions. As the gross error ratio of satellite observations under the overpass increases, the heading error of OB-SPP also increases significantly. In contrast, since the proposed method uses a GNSS observation sequence, the number of available satellite observations is increased, the proportion of faulty satellites is diluted, and faulty satellites are easier to identify and eliminate, so there is no decrease in the accuracy of heading initialization. A similar phenomenon is observed in Fig. 6 (b). However, if the proportion of satellite observation errors is still high in the entire observation sequence, as shown in Fig. 6 (c), the performance of the proposed method will also drop significantly. Nevertheless, it is still more robust than the single-epoch based method due to the averaging effect of multiple epochs. In rare cases, such as around sample 2160 in Fig. 6 (d), the heading initialization accuracy of the proposed method may be lower than that of OB-SPP because most of the satellite observations in the observation sequence are errors. Overall, the proposed method undoubtedly shows the best robustness.

2) *Velocity Error*: Fig. 8 shows the CDF of the velocity error for the three methods using six datasets. RMS of velocity error for the three methods using six datasets are shown in Table V. The average velocity error for RTKLIB and

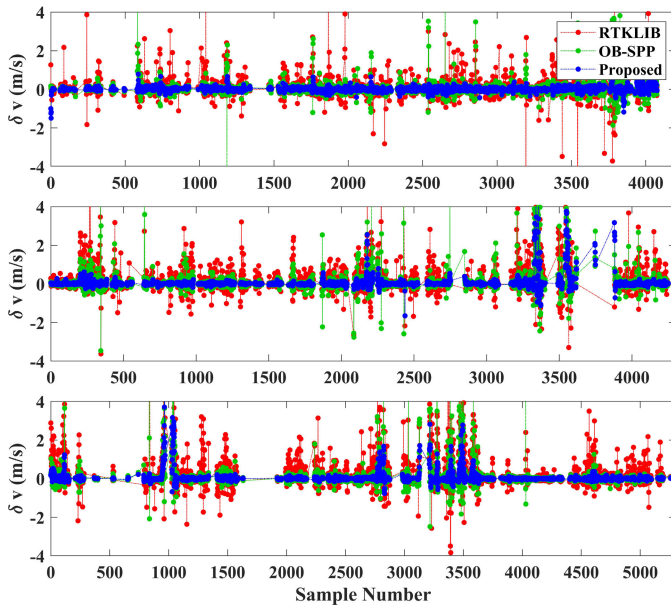


Fig. 7. Velocity error for RTKLIB, OB-SPP, and the proposed method using datasets A1, B1, C1.

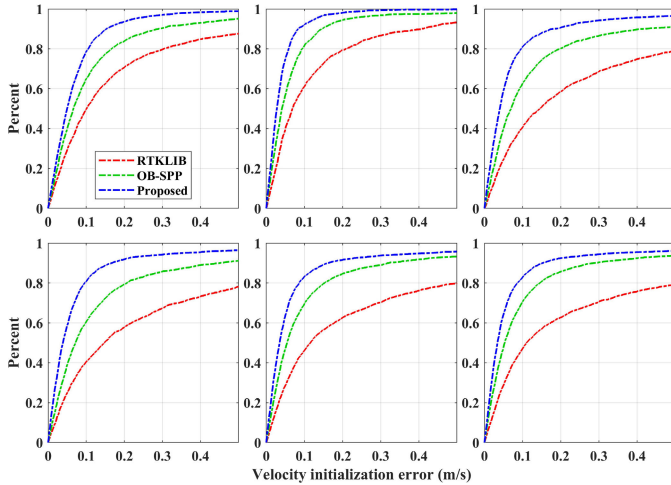


Fig. 8. CDF of velocity error for RTKLIB, OB-SPP, and the proposed method using six datasets.

OB-SPP are 0.80 and 0.51 m/s , respectively. The velocity error for the proposed method using six datasets ranges from 0.07 to 0.44 m/s , and the average velocity error is 0.30 m/s . Compared with the existing methods, the proposed method reduces the velocity error by 62% and 41%, respectively.

Fig. 7 shows the velocity error for the three methods using datasets A1, B1, C1. Similar to heading initialization, the proposed method can effectively suppress the influence of GNSS observation errors and obtain the highest accuracy velocity initialization. The reason is that Doppler observations can directly correct velocity errors and play a greater role in heading initialization than pseudorange observations. Therefore, both heading and velocity initialization have achieved significant accuracy improvements, and the performance of state estimation errors is relatively consistent.

3) *Position Error*: Fig. 10 shows horizontal position error for the three methods using datasets A1, B1, C1. Fig. 9 shows the CDF of the horizontal position error for the three methods

TABLE V
RMS OF VELOCITY ERROR FOR RTKLIB, OB-SPP, AND THE PROPOSED METHOD USING SIX DATASETS (UNIT: m/s)

Dataset	RTKLIB			OB-SPP			Proposed		
	RMS	68%	95%	RMS	68%	95%	RMS	68%	95%
A1	0.68	0.18	0.97	0.39	0.11	0.49	0.19	0.08	0.22
A2	0.35	0.13	0.67	0.21	0.07	0.21	0.07	0.04	0.13
B1	0.78	0.29	1.57	0.61	0.12	0.91	0.40	0.06	0.34
B2	1.28	0.30	1.52	0.63	0.13	0.95	0.44	0.06	0.35
C1	0.86	0.27	1.79	0.64	0.09	0.70	0.35	0.06	0.42
C2	0.86	0.26	1.62	0.60	0.09	0.73	0.36	0.06	0.34
Average	0.80	0.24	1.36	0.51	0.10	0.67	0.30	0.06	0.30

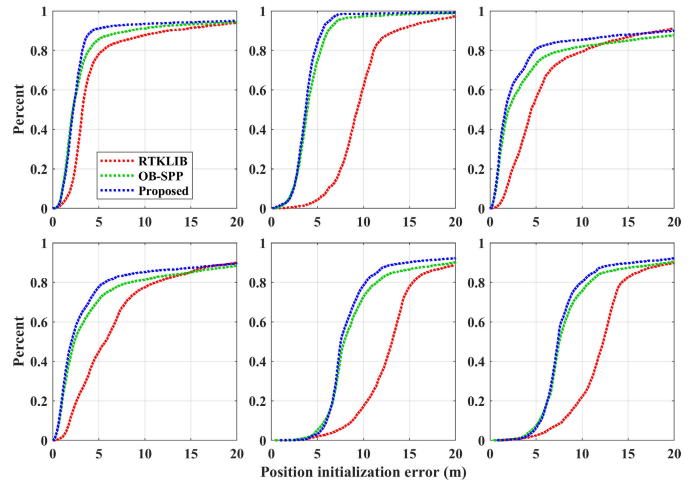


Fig. 9. CDF of horizontal position error for RTKLIB, OB-SPP, and the proposed method using six datasets.

using six datasets. RMS of horizontal position error for the three methods using all datasets are shown in Table V. The average error of horizontal position for RTKLIB and OB-SPP are 14.2 and 12.9 m , respectively. The horizontal position error for the proposed method using six datasets ranges from 5.2 to 13.9 m , and the average horizontal position error is 11.1 m . Compared with the existing methods, the proposed method reduces the horizontal position error by 21% and 14%, respectively. The proposed method does not significantly improve the position initialization accuracy. The reason is that the essence of the proposed method is to use high-precision INS relative pose to suppress pseudorange observation errors in dynamic environments, but it is very dependent on the error distribution characteristics of pseudorange observations. The signal baseband processing method in GNSS receivers usually uses high-intensity filtering to output continuous pseudorange observations in complex urban environments, resulting in very strong time correlation of pseudoranges within a 10-second time window, which limits the benefits of the proposed method.

D. Ablation Experiment

This section mainly discusses the impact of various parameter settings in the proposed algorithm on the accuracy of INS state initialization, including two-step optimization, accelerometer bias estimation and observation sequence length.

TABLE VI

RMS OF HORIZONTAL POSITION ERROR FOR RTKLIB, OB-SPP, AND THE PROPOSED METHOD USING SIX DATASETS (UNIT: M)

Dataset	RTKLIB			OB-SPP			Proposed		
	RMS	68%	95%	RMS	68%	95%	RMS	68%	95%
A1	14.5	4.0	23.5	11.2	3.0	23.9	9.4	2.8	19.7
A2	10.5	10.3	17.4	6.3	4.6	7.2	5.2	4.2	6.3
B1	13.3	6.2	29.3	16.5	4.2	40.5	13.9	3.2	36.5
B2	13.9	7.6	29.5	16.3	4.5	38.5	13.4	3.7	33.0
C1	17.6	14.1	30.9	14.0	9.5	30.6	12.5	8.9	25.9
C2	15.6	13.3	28.6	13.4	8.8	29.4	12.1	8.3	26.0
Average	14.2	9.3	26.5	12.9	5.8	28.3	11.1	5.2	24.6

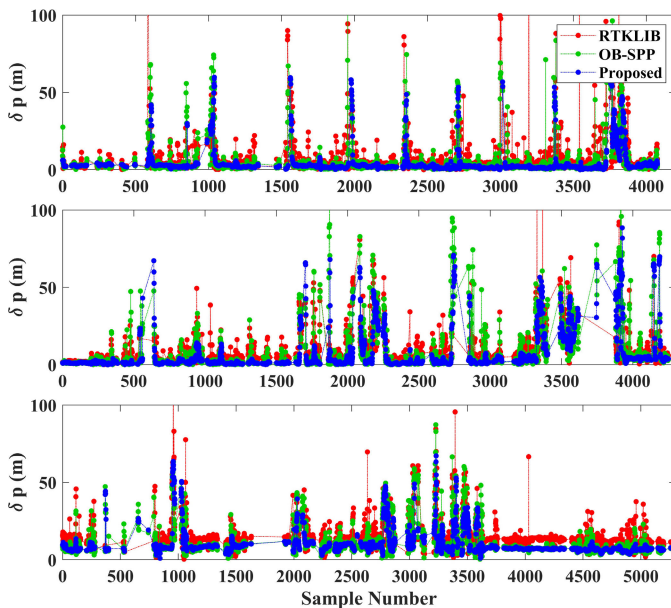


Fig. 10. Horizontal position error for RTKLIB, OB-SPP, and the proposed method using datasets A1, B1 and C1.

1) *Two-Step Optimization*: Fig. 11 shows the CDF of the time consumed by one-step optimization and two-step optimization. One-step optimization is to solve all the parameters to be estimated uniformly. The RMS values for time consumption of one-step and two-step optimization are 76.08 ms and 21.45ms respectively. The proposed two-step optimization strategy reduces the average time consumption by 71.80%. The main reasons include: On the one hand, the complexity of solving the optimization problem can be roughly considered to be proportional to the cube of the state dimension. Solving the low-dimensional state through two-step optimization can effectively reduce the overall complexity. On the other hand, GNSS Doppler has higher accuracy, and the corresponding speed and heading states are more observable. The two-step optimization can achieve the same estimation accuracy with fewer iterations. One-step optimization uses GNSS pseudorange and Doppler at the same time. Due to the large pseudorange observation error and the short vehicle trajectory, the observability of the position is significantly lower, resulting in more iterations and a significant increase in computational complexity.

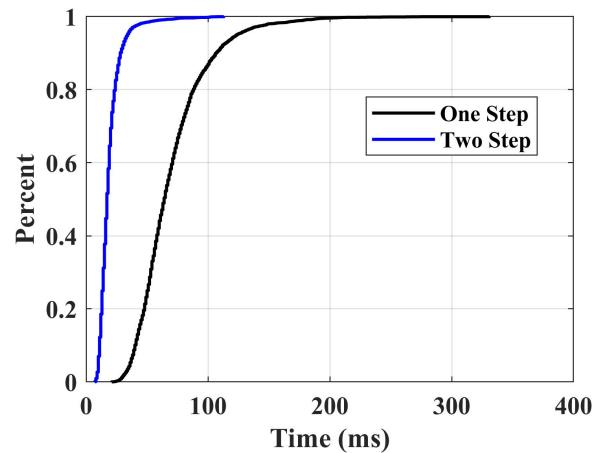


Fig. 11. CDF of the time consumed by one-step optimization and two-step optimization.

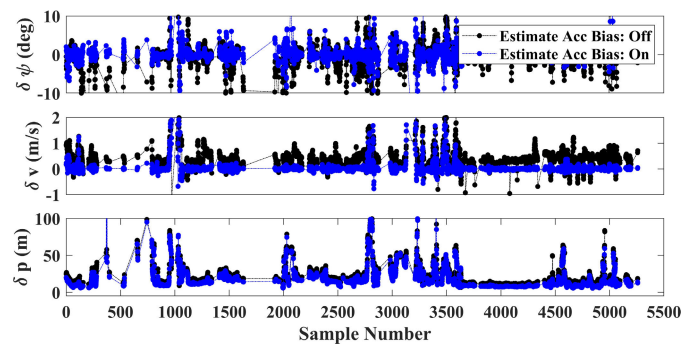


Fig. 12. Effect of accelerometer bias estimation on heading and velocity initialization errors when using dataset C1.

2) *Accelerometer Bias Estimation*: Low-cost MEMS IMUs often exhibit significant accelerometer bias, which directly affects the accuracy of short-term velocity calculations and, in turn, significantly degrades the accuracy of INS state initialization. Unlike gyroscope bias, which can be easily removed using static periodic data, the proposed method incorporates accelerometer bias into the estimated state to remove its effect.

Fig. 12 shows the heading and velocity initialization errors before and after estimating the accelerometer bias using dataset C1. Table VII summarizes the velocity and heading initialization RMSE before and after estimating the accelerometer bias using dataset C1. The velocity initialization error has a systematic bias of 0.4 m/s when the accelerometer bias is present, while the velocity error fluctuates around zero when the accelerometer bias is used as the estimated state. In addition, the heading initialization error is also reduced by estimating the accelerometer bias. Overall, estimating the accelerometer bias reduces the heading and velocity initialization errors by 19% and 38%, respectively.

Fig. 13 shows the estimated x-axis accelerometer bias (along the vehicle's moving direction) versus the reference value (obtained by GNSS/INS integrated navigation solution). The estimated accelerometer bias is very close to the reference value, but the estimated accelerometer bias has significant noise and outliers. The reason is that the accelerometer bias estimation accuracy is related to the Doppler velocity accuracy,

TABLE VII
RMS OF HEADING AND VELOCITY INITIALIZATION ERRORS
WHEN USING DATASET C1

	Velocity (m/s)	Heading (deg)
Acc Bias Estimation (Off)	0.56	3.80
Acc Bias Estimation (On)	0.35	3.07
Error Decrease	38%	19%

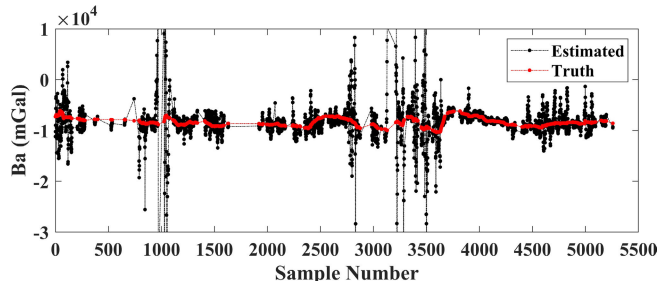


Fig. 13. Comparison of estimated and true x-axis accelerometer bias.

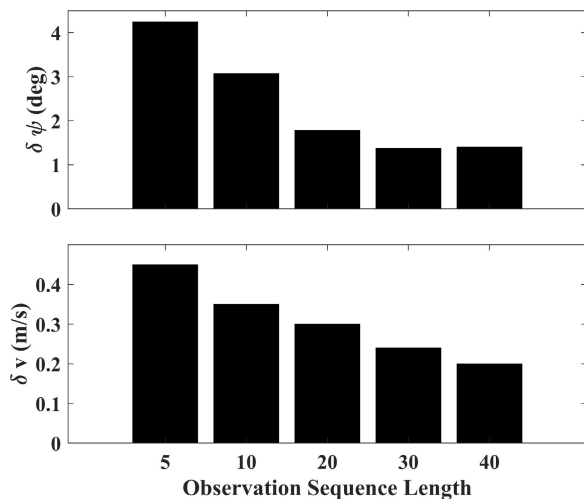


Fig. 14. RMSE of velocity and heading error corresponding to different observation sequence lengths when using dataset C1.

and the Doppler observation error ratio in the sliding window can cause significant fluctuations.

3) *Observation Sequence Length*: The proposed initialization method uses INS to establish the connection between GNSS observations within a preset time window, and achieves robust INS state initialization by increasing the number of available satellite observations and diluting the proportion of faulty satellites. However, observation sequence length (i.e., time window) cannot be extended indefinitely. The reason is that as time increases, small error corrections will also have significant negative effects. At the same time, the extension of the time window will significantly increase the computational load, which contradicts the design goal of fast initialization.

Fig. 14 shows the effect of different observation sequence length on the velocity and heading initialization accuracy when using dataset C1. When the observation sequence length increases from 5 seconds to 30 seconds, the heading initialization error decreases from 4.24° to 1.37° . However, the heading initialization accuracy does not improve with the

increase in time length, and even decreases slightly, because errors such as gyroscope bias become non-negligible at long time scales. In addition, as the observation sequence length increases from 5 seconds to 40 seconds, the speed initialization error decreases from 0.45 m/s to about 0.2 m/s. Considering the INS state initialization response efficiency and estimation accuracy, this study recommends that the observation sequence length be set to 10 to 20 seconds.

V. CONCLUSION

This study proposes a robust INS state initialization method assisted by GNSS pseudorange and Doppler observation sequences for typical urban environments. The proposed method uses the high-precision relative pose generated by INS to construct constraints between GNSS observation sequences, transforms the INS state initialization problem into an optimization problem, and achieves robust and efficient INS state initialization through a two-step optimization solution.

We conducted six route tests in typical urban scenarios, such as under viaducts and urban canyons. The test results show that the proposed method can provide the average error of 2.50° for heading, 0.30 m/s for velocity, and 11.1 m for horizontal position using a 10-second time window, which are reduced by 72%, 41%, and 14% respectively compared with the existing methods. In addition, we discuss the impact of the observation sequence length on the accuracy of INS state estimation and recommend setting the observation sequence length to 10 to 20 seconds in order to achieve a balance between initialization efficiency and accuracy.

This work focuses on fast and robust initialization of INS states in typical urban environments, and has achieved significant performance improvements. In the future, we will try to use this method to improve the robustness of GNSS observations during the navigation phase, so as to achieve continuous and reliable positioning in typical urban environments. Moreover, this method is applicable to any carrier in outdoor scenarios, and we will also try to further verify its performance on carriers such as pedestrians and drones.

REFERENCES

- [1] V. Havyarimana, D. Hanyurwimfura, P. Nsengiyumva, and Z. Xiao, "A novel hybrid approach based-SRG model for vehicle position prediction in multi-GPS outage conditions," *Inf. Fusion*, vol. 41, pp. 1–8, May 2018.
- [2] C. Gao, G. Wang, W. Shi, Z. Wang, and Y. Chen, "Autonomous driving security: State of the art and challenges," *IEEE Internet Things J.*, vol. 9, no. 10, pp. 7572–7595, May 2022.
- [3] V. Havyarimana, Z. Xiao, T. Semong, J. Bai, H. Chen, and L. Jiao, "Achieving reliable intervehicle positioning based on redheffer weighted least squares model under multi-GNSS outages," *IEEE Trans. Cybern.*, vol. 53, no. 2, pp. 1039–1050, Feb. 2023.
- [4] Q. Chen, H. Lin, J. Kuang, Y. Luo, and X. Niu, "Rapid initial heading alignment for MEMS land vehicular GNSS/INS navigation system," *IEEE Sensors J.*, vol. 23, no. 7, pp. 7656–7666, Apr. 2023.
- [5] Z. F. Syed, P. Aggarwal, X. Niu, and N. El-Sheimy, "Civilian vehicle navigation: Required alignment of the inertial sensors for acceptable navigation accuracies," *IEEE Trans. Veh. Technol.*, vol. 57, no. 6, pp. 3402–3412, Nov. 2008.
- [6] P. D. Groves, R. J. Handley, and S. T. Parker, "Vehicle heading determination using only single-antenna GPS and a single gyro," in *Proc. 22nd Int. Tech. Meeting Satell. Division Inst. Navigat. (ION GNSS)*, Sep. 2009, pp. 1775–1784.

- [7] S. Han and J. Wang, "A novel initial alignment scheme for low-cost INS aided by GPS for land vehicle applications," *J. Navigat.*, vol. 63, no. 4, pp. 663–680, Oct. 2010.
- [8] L. Chang and B. Hu, "Robust initial attitude alignment for SINS/DVL," *IEEE/ASME Trans. Mechatronics*, vol. 23, no. 4, pp. 2016–2021, Aug. 2018.
- [9] X. Xu, Y. Sun, J. Gui, Y. Yao, and T. Zhang, "A fast robust in-motion alignment method for SINS with DVL aided," *IEEE Trans. Veh. Technol.*, vol. 69, no. 4, pp. 3816–3827, Apr. 2020.
- [10] Y. Huang, Y. Zhang, and X. Wang, "Kalman-filtering-based in-motion coarse alignment for odometer-aided SINS," *IEEE Trans. Instrum. Meas.*, vol. 66, no. 12, pp. 3364–3377, Dec. 2017.
- [11] A. Wahdan, J. Georgy, W. F. Abdelfatah, and A. Noureldin, "Magnetometer calibration for portable navigation devices in vehicles using a fast and autonomous technique," *IEEE Trans. Intell. Transp. Syst.*, vol. 15, no. 5, pp. 2347–2352, Oct. 2014.
- [12] R. Sun, Q. Cheng, and J. Wang, "Precise vehicle dynamic heading and pitch angle estimation using time-differenced measurements from a single GNSS antenna," *GPS Solutions*, vol. 24, no. 3, p. 84, Jul. 2020.
- [13] P. D. Groves, "Principles of GNSS, inertial, and multisensor integrated navigation systems, 2nd edition [Book review]," *IEEE Aerosp. Electron. Syst. Mag.*, vol. 30, no. 2, pp. 26–27, Feb. 2015.
- [14] Q. Chen, H. Lin, R. Guo, and X. Niu, "Rapid and accurate initial alignment of the low-cost MEMS IMU chip dedicated for tilted RTK receiver," *GPS Solutions*, vol. 24, no. 4, p. 119, Oct. 2020.
- [15] R. G. Brown and P. W. McBurney, "Self-contained GPS integrity check using maximum solution separation," *Navigation*, vol. 35, no. 1, pp. 41–53, Mar. 1988.
- [16] L. Chang and K. Li, "Unified form for the robust Gaussian information filtering based on M-estimate," *IEEE Signal Process. Lett.*, vol. 24, no. 4, pp. 412–416, Apr. 2017.
- [17] E.-H. Shin and N. El-Sheimy, "An unscented Kalman filter for in-motion alignment of low-cost IMUs," in *Proc. PLANS Position Location Navigat. Symp.*, Oct. 2004, pp. 273–279.
- [18] D. Wang, H. Lv, and J. Wu, "In-flight initial alignment for small UAV MEMS-based navigation via adaptive unscented Kalman filtering approach," *Aerosp. Sci. Technol.*, vol. 61, pp. 73–84, Feb. 2017.
- [19] M. Wu, Y. Wu, X. Hu, and D. Hu, "Optimization-based alignment for inertial navigation systems: Theory and algorithm," *Aerosp. Sci. Technol.*, vol. 15, no. 1, pp. 1–17, Jan. 2011.
- [20] Y. Wu and X. Pan, "Velocity/position integration formula part I: Application to in-flight coarse alignment," *IEEE Trans. Aerosp. Electron. Syst.*, vol. 49, no. 2, pp. 1006–1023, Apr. 2013.
- [21] L. Chang, J. Li, and K. Li, "Optimization-based alignment for strapdown inertial navigation system: Comparison and extension," *IEEE Trans. Aerosp. Electron. Syst.*, vol. 52, no. 4, pp. 1697–1713, Aug. 2016.
- [22] Y. Wu, J. Wang, and D. Hu, "A new technique for INS/GNSS attitude and parameter estimation using online optimization," *IEEE Trans. Signal Process.*, vol. 62, no. 10, pp. 2642–2655, May 2014.
- [23] Y. Wei, H. Li, and M. Lu, "Carrier Doppler-based initial alignment for MEMS IMU/GNSS integrated system under low satellite visibility," *GPS Solutions*, vol. 25, no. 3, p. 90, Jul. 2021.
- [24] Y. Huang, Y. Zhang, and L. Chang, "A new fast in-motion coarse alignment method for GPS-aided low-cost SINS," *IEEE/ASME Trans. Mechatronics*, vol. 23, no. 3, pp. 1303–1313, Jun. 2018.
- [25] Y. Huang, Z. Zhang, S. Du, Y. Li, and Y. Zhang, "A high-accuracy GPS-aided coarse alignment method for MEMS-based SINS," *IEEE Trans. Instrum. Meas.*, vol. 69, no. 10, pp. 7914–7932, Oct. 2020.
- [26] Q. Zhang, S. Li, Z. Xu, and X. Niu, "Velocity-based optimization-based alignment (VBOBA) of low-end MEMS IMU/GNSS for low dynamic applications," *IEEE Sensors J.*, vol. 20, no. 10, pp. 5527–5539, May 2020.
- [27] T. Zhang, S. Liu, Q. Chen, X. Feng, and X. Niu, "Carrier-phase-based initial heading alignment for land vehicular MEMS GNSS/INS navigation system," *IEEE Trans. Instrum. Meas.*, vol. 71, pp. 1–13, 2022.
- [28] Y. Wu, C. He, and G. Liu, "On inertial navigation and attitude initialization in polar areas," *Satell. Navigat.*, vol. 1, no. 1, p. 4, Jan. 2020.
- [29] Q. Chen, Q. Zhang, and X. Niu, "Estimate the pitch and heading mounting angles of the IMU for land vehicular GNSS/INS integrated system," *IEEE Trans. Intell. Transp. Syst.*, vol. 22, no. 10, pp. 6503–6515, Oct. 2021.
- [30] S. O. H. Madgwick, A. J. L. Harrison, and R. Vaidyanathan, "Estimation of IMU and MARG orientation using a gradient descent algorithm," in *Proc. IEEE Int. Conf. Rehabil. Robot.*, Jun. 2011, pp. 1–7.
- [31] R. Mahony, T. Hamel, and J.-M. Pfimlin, "Nonlinear complementary filters on the special orthogonal group," *IEEE Trans. Autom. Control*, vol. 53, no. 5, pp. 1203–1218, Jun. 2008.
- [32] J. Kuang, T. Li, and X. Niu, "Magnetometer bias insensitive magnetic field matching based on pedestrian dead reckoning for smartphone indoor positioning," *IEEE Sensors J.*, vol. 22, no. 6, pp. 4790–4799, Mar. 2022.
- [33] P. G. Savage, "Strapdown inertial navigation integration algorithm design part 1: Attitude algorithms," *J. Guid., Control, Dyn.*, vol. 21, no. 1, pp. 19–28, Jan. 1998.
- [34] T. Takasu and A. Yasuda, "Development of the low-cost RTK-GPS receiver with an open source program package RTKLIB," in *Proc. Int. Symp. GPS/GNSS*, vol. 1, Jeju-si, South Korea, 2009, pp. 1–6.
- [35] J. Nocedal and S. J. Wright, *Numerical Optimization*. Cham, Switzerland: Springer, 1999.
- [36] S. Cao, X. Lu, and S. Shen, "GVINS: Tightly coupled GNSS-visual-inertial fusion for smooth and consistent state estimation," *IEEE Trans. Robot.*, vol. 38, no. 4, pp. 2004–2021, Aug. 2022.